Eur Radiol (2011) 21:246–255
DOI 10.1007/s00330-010-1929-x

MOLECULAR IMAGING

Diagnostic accuracy of whole-body MRI/DWI image fusion for detection of malignant tumours: a comparison with PET/CT

Michael A. Fischer · Daniel Nanz · Thomas Hany · Caecilia S. Reiner · Paul Stolzmann · Olivio F. Donati · Stefan Breitenstein · Paul Schneider · Dominik Weishaupt · Gustav K. von Schulthess · Hans Scheffel

Received: 6 May 2010 / Revised: 15 July 2010 / Accepted: 21 July 2010 / Published online: 18 August 2010

Abstract
Objective To prospectively evaluate the diagnostic accuracy of whole-body T2-weighted (wbT2), whole-body diffusion-weighted imaging (wbDWI) and wbT2/wbDWI image fusion for malignant tumour detection compared with PET/CT.
Methods Sixty-eight patients (44 men; 60±14 years) underwent PET/CT for staging of malignancy and were consecutively examined by 1.5-Tesla MRI including wbT2 and wbDWI. Two radiologists independently assessed wbDWI, wbT2, wbT2 + wbDWI (side-by-side) and wbT2 + wbDWI + wbT2/wbDWI image fusion for the presence of malignancy. PET/CT served as a reference standard.
Results PET/CT revealed 374 malignant lesions in 48/64 (75%) patients. Detection rates and positive predictive value (PPV) of wbT2 and wbDWI alone were 64% and 84%, and 57% and 93%, respectively. Detection rates and PPV of wbT2 and wbDWI for side-by-side analysis without and with fused images were 72% and 89%, and 74% and 91%, respectively. The detection rate was significantly higher with side-by-side analysis and fused image analysis compared with wbT2 and wbDWI alone ($p=.0159$; $p<.0001$). There was no significant difference between fused image interpretation and side-by-side analysis.
Conclusions WbDWI allows detection of malignant lesions with a similar detection rate to wbT2. Side-by-side analysis of wbT2 and wbDWI significantly improves the overall detection rate and fused image data provides no added value.

Keywords Diffusion-weighted imaging · Magnetic resonance imaging · Whole body imaging · Positron emission computed tomography · Image fusion

M. A. Fischer · D. Nanz · C. S. Reiner · P. Stolzmann · O. F. Donati · H. Scheffel (✉)
Institute of Diagnostic and Interventional Radiology, University Hospital Zurich, Raemistr. 100, 8091 Zurich, Switzerland
e-mail: hans.scheffel@usz.ch

T. Hany · G. K. von Schulthess
Institute of Nuclear Medicine, University Hospital Zurich, Zurich, Switzerland

S. Breitenstein · P. Schneider
Clinic of Visceral and Transplant Surgery, University Hospital Zurich, Zurich, Switzerland

D. Weishaupt
Institute of Radiology, Triemli Hospital, Zurich, Switzerland

Introduction

Integrated positron emission tomography (PET)/computed tomography (CT) plays a central role in medical imaging for detection and staging of cancer [1, 2].

Over the past decade whole-body magnetic resonance imaging (MRI) has become applicable for evaluation of malignancy because of advances in imaging technology [3, 4]. Whole-body T2-weighted imaging (wbT2) with fat suppression and short tau inversion recovery (STIR) demonstrate the most frequently applied sequences because of good anatomical image information [5]. Compared with PET/CT, however, assessment of malignant tumour disease with MRI is mainly based on morphological changes [6], whereas functional changes are not be visualised.

Integration of functional data in terms of whole-body (wb) diffusion-weighted imaging (DWI) was first enabled by Takahara et al. [7], who developed wbDWI under free breathing (whole-body diffusion-weighted imaging with background body signal suppression; DWIBS). As most tumours are not only characterised by pathological glucose metabolism but also restricted diffusion because of higher tissue cellularity [8], wbDWI can be useful in the detection of malignancy similar to PET imaging [9]. However, wbDWI is accompanied by low spatial-resolution and therefore restricted anatomical information [10]. Similar to PET/CT imaging, where CT provides detailed morphological information that increases diagnostic accuracy compared with PET alone [11], combined assessment of wbT2 and wbDWI may improve evaluation of malignant tumour disease [12].

The aim of this study was to evaluate the ability of wbT2 and wbDWI for the detection of malignant tumours and to evaluate the additional value of wbT2/wbDWI image fusion.

Materials and methods

Patients

This prospective study was approved by the local ethics committee. Written informed consent was obtained from all patients according to the Declaration of Helsinki guidelines.

Between January and November 2009, 68 patients with malignancies (44 men; 24 women; mean age 60±14 years), who were referred for staging of malignant tumour disease by means of PET/CT for clinical reasons, consecutively underwent an additional wbT2 and wbDWI examination. WbT2 and wbDWI was performed within 10 days before or after PET/CT.

Exclusion criteria were chemotherapy and radiotherapy between PET/CT and MRI, and denied informed consent (n=0) as well as MRI-related contraindications (i.e. claustrophobia or metallic implants).

Four patients were excluded because of chemotherapy (n=3) and combined radio-/chemotherapy (n=1) between the two examinations. Thus, the study was conducted in 64 patients, 42 men (mean age, 60±13 years; range, 18–80 years) and 22 women (mean age, 59±17 years; range, 20–78 years), with a overall mean age of 60±14 years; range 18–80 years.

Underlying tumour disease was oesophagogastrointestinal carcinoma in 31 patients (48%), cholangiocarcinoma in 14 patients (22%), lymphoma in 11 patients (17%), pancreatic carcinoma in five patients (8%) and melanoma in three patients (5%). Eighteen patients (28%) underwent chemotherapy, six patients (9%) combined chemo- and radiotherapy, and one patient had radiotherapy (2%) before the imaging protocol, respectively (Table 1).

PET/CT imaging

Imaging with PET/CT was acquired using [18]F-fluorodeoxyglucose (^{18}F-FDG) on a combined PET-CT in-line system (Discovery VCT; GE HealthCare, Waukesha, WI, USA). ^{18}F-FDG (350 MBq) was injected 60 min before PET imaging when glucose levels were within the normal range (range, 80–120 mg/dL [4.4–6.7 mmol/L]) after at least 4 h of fasting. Whole-body (head to knee) low-dose CT for attenuation correction was performed with acquisition parameters of 40 mAs, 140 kV, 0.5 s/ rotation, 4.25-mm slice thickness, 867-mm mean image length, pitch of 1.7, and 22.5-s data acquisition time. Emission PET was acquired within 1 min of CT with the patient in the same position using 8–9 incremental table positions from head to knees and a matrix of 128×128. In 20/68 (29%) of the patients an additional, clinically indicated, abdominal contrast-enhanced CT was performed after injection of 100 mL of iopromide intravenous contrast agent (Visipac 320, iodum 320 mg/mL Sinclair & Rush, Inc., MO, USA) followed by 20 mL saline solution. Imaging parameters were 120 kV, 100–200 mAs attenuation-based tube current modulation (auto mAs), a slice thickness of 3.75 mm and a

Table 1 Patient demographics

Male patients	42 (66%)
Female patients	22 (34%)
Age (years)	60±14 (18–80)
Primary malignancy	
Oesophagogastrointestinal cancer	31 (48%)
Oesophageal carcinoma	9 (14%)
Gastric carcinoma	7 (11%)
Colorectal carcinoma	15 (23%)
Cholangiocellular carcinoma	14 (22%)
Lymphoma	11 (17%)
Hodgkin lymphoma	2 (18%)
B-cell lymphoma	6 (55%)
T-cell lymphoma	3 (27%)
Pancreatic carcinoma	5 (8%)
Melanoma	3 (5%)
Medical history	
Primary staging	45 (70%)
Resected primary malignancy	14 (22%)
Re-staging after therapy	19 (30%)
Chemotherapy	18 (28%)
Radiotherapy	1 (2%)
Combined radio-/Chemotherapy	6 (9%)

pitch of 1.7. The total average imaging time for PET/CT was 28±6 min.

Magnetic resonance imaging

All patients underwent MRI at 1.5-T (Signa Echospeed EXCITE HDx, GE Healthcare, Waukesha, WI, USA) in a supine position with arms overhead or if not possible parallel to the body and feet first. For signal detection of the head and lower extremity the integrated scanner coil was used, whereas thorax and abdomen were covered through an eight-element body phased-array coil allowing for parallel imaging. Overview and calibration MR images for surface-coil sensitivity as well as calibration imaging for upper and lower body-array coils were acquired in expiration.

WbDWI was performed under free breathing using an axial single-shot echo planar imaging sequence and motion probing gradients in superior/inferior direction with *b*-values of 0 and 700 s/mm^2 for background body signal suppression. For fat suppression a chemical shift selective saturation pulse ("fat-sat") was used. WbDWI parameters: Repetition time (TR)/Echo Time (TE): 6200/68.6 msec; image matrix: 128×128; field of view: 480×432 mm (axial); slice thickness: 7 mm; spacing: 1 mm; number of excitations (NEX): 6. The total average imaging time for WbDWI was 22±2 min.

WbT2 was acquired corresponding to each wbDWI section using an axial steady state free precession gradient echo sequence (fast imaging employing steady state acquisition; FIESTA) with breathing triggering in thorax and abdomen. WbT2 parameters: TR/TE: 4.4/2.0 ms, inversion time: 200 ms; image matrix: 288×256; field of view: 480×432 mm (axial); slice thickness: 7 mm; spacing: 1 mm; NEX: 1. Total average imaging time for wbT2 was 19±2 min.

Image post-processing

All MRI and PET/CT images were interpreted at a standard workstation (AW4.3; GE Medical Systems). DWI data were separated with two different *b*-values (b = 0 s/mm^2; b = 700 s/mm^2) yielding 2×7 datasets for each patient. Afterwards, T2 and DWI datasets were reformatted to a whole body image (wbT2 and wbDWI) eliminating the overlaps between sets performed by an investigator who was not involved in data analysis. Apparent diffusion coefficient (ADC) maps were generated.

For image registration and fusion a software prototype ("Multimodality", AW4.3; GE Healthcare) was used to fuse the wbT2 and the b = 700 s/mm^2 wbDWI images. This software enables automatic propagation of rigid registration across series acquired in the same examination based on three registration methods: automatic, manual and landmark-based. In our study, wbT2 and the b = 700 s/mm^2 wbDWI images were fused automatically because of co-registered acquisition of wbT2 and wbDWI source images. WbDWI data image information was displayed on the fused images in an inverted colour scale equal to that used for PET/CT fusion.

Data analysis

PET/CT

Image interpretation was performed in consensus by two radiologists experienced in nuclear oncology body imaging. Both readers were blinded to MRI results. Attenuation-corrected PET images, low-dose CT images, and co-registered fused images were displayed and analysed together. If available, contrast-enhanced CT was included in PET/CT analysis. Malignant lesions were diagnosed when abnormal focal FDG-uptake, observed on PET images corresponded to an abnormal mass on CT. Abnormal focal FDG uptake was considered a FDG uptake higher than two times the mean liver standard uptake value in the right hepatic lobe, which was determined normal background 18F-FDG activity. In case of diffuse abnormal liver uptake, left ventricular blood pool was used as a reference. Pathologic FDG uptake without corresponding CT abnormality was considered as malignant lesion if lesion size was greater 2 cm in diameter for accurate measurement or, for smaller lesions, if any other reasons like artefacts or focal inflammation could be ruled out as reason for abnormal FDG-uptake [13]. Lymph nodes with increased glucose uptake were deemed positive for metastatic spread even if they were smaller than 1 cm in short-axis diameter. Conversely, lymph nodes with no detectable tracer uptake were deemed negative for metastatic spread, even if they were larger than 1 cm in the short-axis diameter. Lung lesions were considered malignant because of morphological issues used in daily routine even though no increased glucose uptake was present.

Magnetic resonance imaging

Two other independent radiologists, not involved in PET/CT data evaluation, performed image interpretation prospectively. Both readers were blinded to PET/CT results as well as all clinical information except the origin of the primary tumour.

In the first session, readers interpreted wbDWI alone. In the second reading session after 10–14 days, wbT2 datasets were interpreted alone. In the third reading session after another 10–14 days wbT2 + wbDWI (side-by-side) datasets were analysed. All images, including fused images were evaluated together (wbT2 + wbDWI + wbT2/wbDWI fused images) in a

fourth reading session after another 10–14 days. Reading order of datasets was randomised. Concerning cases of disagreement, a consensus reading of both readers by discussion was appended 7 days after the initial data read-out. WbDWI images were interpreted using the mulitplanar reformation tool ("reformat") allowing the assessment of axial source images. No maximum intensity projection images were evaluated. WbT2 and fused images were analysed in axial plane using the viewer function of the AW4.3. Malignant lesions were documented according to their exact anatomical location and slice position for each image.

wbDWI

For wbDWI any distinct focus on b = 700 s/mm^2 images with increased signal intensity compared with the intensity of the surrounding tissue was considered a malignant lesion, if ADC values of the lesion were lower than ADC values of the healthy surrounding tissue. If ADC values were equal or greater than the surrounding tissue indicating a T2-shine through effect, lesions were considered benign. Accordingly lymph nodes were considered malignant if ADC values showed restricted or increased diffusion regardless of their size and morphology [14].

wbT2

Any lesion was classified as malignant if an intermediate to hyperintense signal intensity in comparison to skeletal muscle and an expansive growth pattern was present [15] except tumorous lesions in melanoma patients, which were also considered malignant if a hypointense signal was present. Enlarged lymph nodes were considered to be malignant based on measurement of the short axis diameter with cut-off values of >10 mm for cervical, mediastinal and retroperitoneal lymph nodes, >8 mm for intraperitoneal lymph nodes, >11 mm for pelvic lymph nodes and >12 mm for inguinal lymph nodes [16, 17].

Side-by-side analysis and fused images

Side-by-side analysis and interpretation of fused images consisted of a combination of wbT2 and wbDWI evaluation. Lesions were rated as malignant according to the morphological features on wbT2 and to the functional features on wbDWI as mentioned above. Any lesion was rated as positive for malignancy, if the lesion was interpreted as malignant in one of the two sequences.

Statistical analysis

Variables were described as mean±standard deviation or as frequencies and percentages.

Inter-observer agreement was assessed by using *k* statistics and interpreted as follows: A *k*-value greater than 0.81 corresponded to very good agreement, a *k*-value of 0.61 to 0.80 corresponded to good interobserver agreement, a *k*-value of 0.41 to 0.60 corresponded to moderate interobserver agreement, and a *k*-value of 0.21 to 0.40 corresponded to poor interobserver agreement. McNemar's test was used to test for significant differences in rates of immediate interobserver agreement achieved by different dataset evaluations.

Data of the consensus readings was used to evaluate lesion-based detection rates as well as patient-based diagnostic accuracy for wbT2 and wbDWI alone as well as for side-by-side analysis and fused images. For lesion-based analysis, detected lesions were classified as being in the lymph nodes, liver, and lung reflecting the major sites of malignancy. All lesions detected outside those locations were summarised as "others" and evaluated separately.

Detection rates as well as patient-based sensitivity, specificity and accuracy were calculated from χ^2 tests of contingency, and 95% confidence intervals (CI) were calculated from binomial expression.

McNemar's test was used to test for significant differences in lesion-based detection rates and patient-based diagnostic accuracy. *P* values <0.05 were considered statistically significant for all tests. All statistical analyses were performed using commercially available software (SPSS, release 17.0, Chicago, IL, USA).

Results

Patients

All patients underwent MRI as well as PET/CT without adverse events. MRI in the supine position with the arms overhead was tolerated by 33 of 64 (52%) patients, whereas 31 of 64 (48%) did not tolerate the overhead position and the arms had to be placed parallel to the body. In PET/CT all patients (64/64; 100%) tolerated the examination with their arms in the overhead position. Diagnostic image quality was achieved in all patients for wbDWI, wbT2 , fused images, and PET/CT (Figs. 1, 2).

PET/CT

In total, PET/CT revealed 374 malignant lesions in 48/64 (75%) patients. Most malignant lesions were detected in lymph nodes (*n*=153), liver (*n*=107) and lung (*n*=72). Forty-two lesions were present in "other" locations including soft tissue (*n*=11), bone (*n*=11), gastrointestinal tract (*n*=6), kidneys (*n*=4), central nervous system (*n*=4), pancreas (*n*=2), spleen (*n*=2) and adrenal glands (*n*=2).

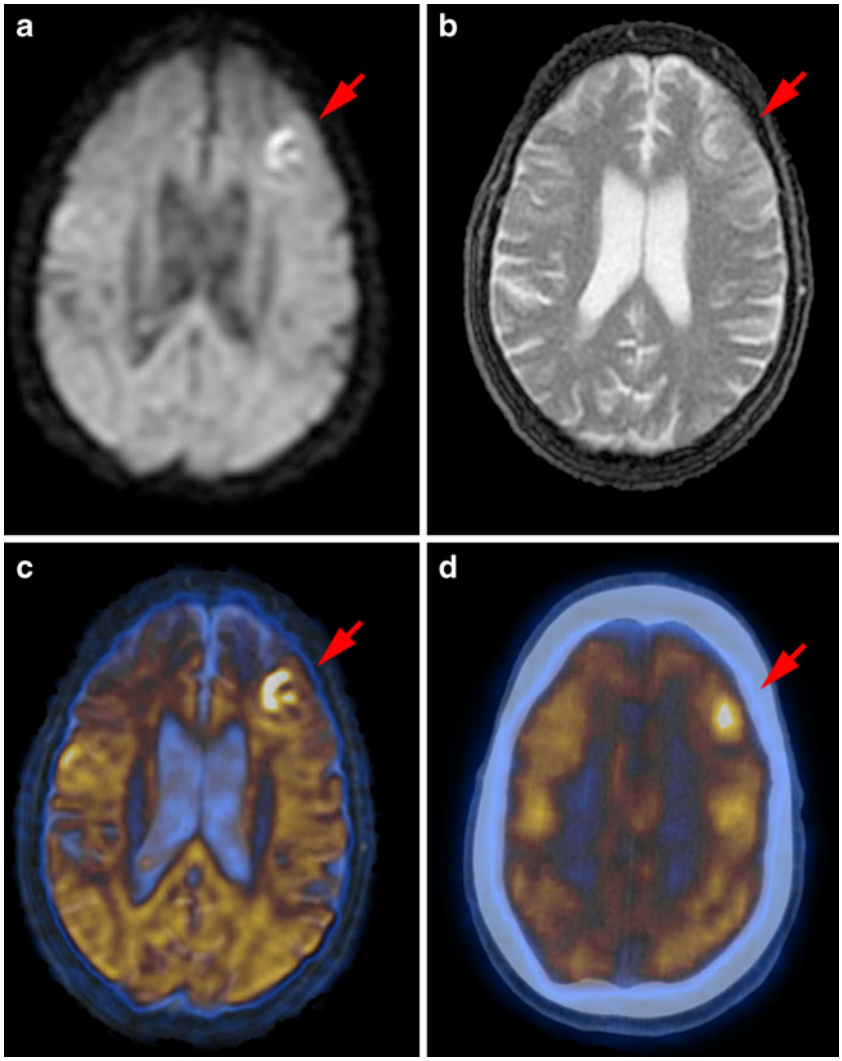

Fig. 1 A 74-year-old male patient with brain metastases from a melanoma. WbDWI (**a**) and wbT2 (**b**) images showed the tumour in the left frontal lobe. Additionally, fused image (**c**) data interpretation allowed the detection of this lesion compared to the PET/CT images (**d**) which served as the reference standard

wbDWI

Inter-observer agreement for analysis of wbDWI was good (k=0.75).

Overall wbDWI detected 238/374 (64%) malignant lesions. Detection rates yielded 109/153 (71%) malignant lymph nodes, 98/107 (92%) liver lesions, 14/72 (19%) lung lesions, and 17/42 (40%) "other" lesions (Table 2). 46/284 (16%) lesions were regarded as false-positive lesions.

Patient based diagnostic accuracy of wbDWI for detection of malignant lesions yielded a sensitivity of 88% (95% CI: 77–97; 42/48), a specificity of 69% (95% CI: 42–94; 11/16), and an accuracy of 83% (95% CI: 72–92; 53/64) using PET/CT as a reference standard (Table 3).

wbT2

Inter-observer agreement for analysis of wbT2 was very good (k=0.84) and significant better than with wbDWI (p<.0001).

In total, wbT2 detected 213/374 (57%) malignant lesions including 99/153 (65%) lymph nodes, 82/107 (77%) liver lesions, 14/72 (19%) lung lesions, and 18/42 (43%) "other" lesions (Table 2). 17/230 (7%) lesions were regarded as false-positive lesions. No significant difference was observed in overall detection rate between wbT2 and wbDWI (p=.07). Diagnostic accuracy of wbT2 for detection of malignant lesions per patient yielded a sensitivity of 85% (95% CI: 74–96; 41/48), a specificity of 88% (95% CI: 68–100; 14/16), and an accuracy of 86% (95% CI: 76–95; 55/64; Table 3) using PET/CT as a reference standard. No significant difference compared to wbDWI (p=.99) was present.

Side-by-side analysis

Inter-observer agreement for side-by-side analysis of wbT2 and wbDWI was very good (k=0.83) with no significant difference to wbT2 (p=.40) but significant difference to wbDWI (p<.0001)

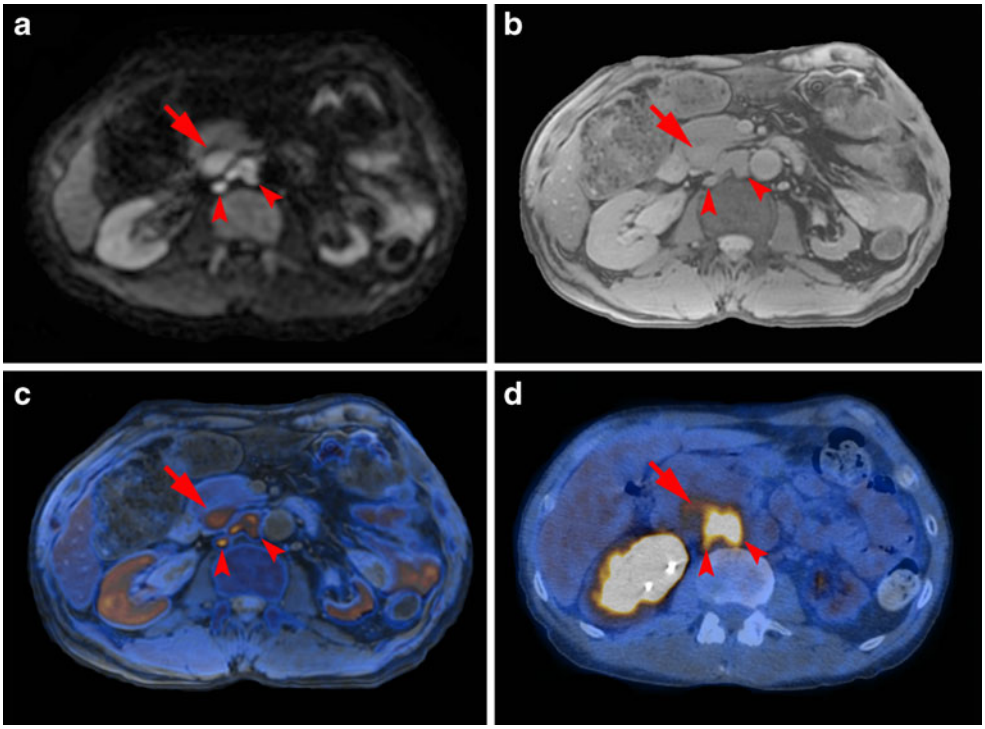

Fig. 2 A 35-year-old male patient with retroperitoneal lymph node metastases from colorectal cancer. **a** WbDWI correctly depicted three retroperitoneal lymph node metastases (*arrows*). **b** WbT2 also depicted the two para-aortic lymph node metastases and the enlarged lymph node dorsal to the pancreatic head (*arrows*). Both side-by-side analysis (**a**+**b**) and image fusion (**c**) allow comprehensive assessment of tumour spread in comparison to PET/CT (**d**)

Side-by-side analysis yielded a total of 270/374 (72%) malignant lesions including 125/153 (82%) malignant lymph nodes, 97/107 (91%) liver lesions, 24/72 (33%) lung lesions, and 24/42 (57%) "other" lesions (Table 2). 32/302 (11%) lesions were regarded as false-positive lesions. Overall detection rate of side-by-side analysis was signif-

Table 2 Lesion-based diagnostic accuracy for detection of malignant lesions using PET/CT as the reference standard

	Detection rate	Positive predictive value
wbDWI	63.6% (58–68;238/374)	83.8% (79–88;238/284)
Lymph node	71.2% (63–78;109/153)	85.8% (79–92;109/127)
Liver	91.5% (85–97;98/107)	86.7% (80–93;98/113)
Lung	19.4% (9–29;14/72)	93.3% (77–100;14/15)
Other	40.4% (24–56;17/42)	58.6% (38–78;17/29)
wbT2	56.9% (51–62;213/374)	92.6% (89–96;213/230)
Lymph node	64.7% (56–72;99/153)	93.3% (88–98;99/106)
Liver	76.6% (68–85;82/107)	90.1% (83–96;82/91)
Lung	19.4% (9–29;14/72)	100% (96–100;14/14)
Other	42.8% (26–59;18/42)	94.7% (82–100;18/19)
Side-by-side*	72.1% (67–76;270/374)	89.4% (85–93;270/302)
Lymph node	81.6% (75–88;125/153)	92.5% (87–97;125/135)
Liver	90.6% (84–96;97/107)	85.8% (78–92;97/113)
Lung	33.3% (21–44;24/72)	96% (86–100;24/25)
Other	57.1% (40–73;24/42)	82.7% (67–98;24/29)
Fused images**	73.5% (68–78;275/374)	90.7% (87–94;275/303)
Lymph node	84.3% (78–90;129/153)	95.5% (91–99;129/135)
Liver	90.6% (84–96;97/107)	84.3% (77–91;97/115)
Lung	34.7% (23–46;25/72)	96.1% (86–100;25/26)
Other	57.1% (40–73;24/42)	88.8% (75–100;24/27)

*Significant difference compared with both wbDWI ($p<0.05$) and wbT2 ($p<0.0001$); **significant difference compared with both wbDWI ($p<0.001$) and wbT2 ($p<0.0001$)

Numbers in parentheses are 95% confidence intervals and absolute numbers

wbDWI whole-body diffusion-weighted Imaging, *wbT2* whole-body T2-weighted Imaging, side-by-side: wbDWI + wbT2; fused images: wbDWI + wbT2 + wbDWI/wbT2 fused images

Other: intestinal and urogenital tract, spleen, soft tissue, skeletal system, central nervous system

Table 3 Patient-based diagnostic accuracy for detection of malignant lesions using PET/CT as the reference standard

	Diagnostic accuracy		
	Sensitivity (%)	Specifity (%)	Accuracy (%)
wbDWI	88% (77–97;42/48)	69% (42–94;11/16)	83% (72–92;53/64)
wbT2	85% (74–96;41/48)	81% (58–100;13/16)	84% (74–94;54/64)
Side-by-side	96% (89–100;46/48)	75% (50–99;12/16)	91% (82–98;58/64)
Fused images	96% (89–100;46/48)	75% (50–99;12/16)	91% (82–98;58/64)

Numbers in parentheses are 95% confidence intervals and absolute numbers; *wbDWI* whole-body diffusion-weighted Imaging, *wbT2* whole-body T2-weighted Imaging, side-by-side: wbDWI + wbT2; fused images: wbDWI + wbT2 + wbDWI/wbT2 fused images

icant higher compared to both wbDWI ($p<.05$) and wbT2 ($p<.0001$) (Figs. 3, 4).

Diagnostic accuracy of side-by-side analysis on a per patient basis showed a sensitivity of 96% (95% CI: 89–100; 46/48), a specificity of 75% (95% CI: 50–99; 12/16), and an accuracy of 91% (95% CI: 82–98; 58/64, Table 3) using PET/CT as a reference standard. Regarding diagnostic accuracies, there were neither significant differences between side-by-side and wbT2 ($p=.42$) nor between side-by-side and wbDWI ($p=.30$), respectively.

Fused images

Inter-observer agreement for analysis of fused images was very good ($k=0.83$) with no significant difference to both wbT2 and side-by-side analysis.

Assessment of fused images revealed a total of 275/374 (74%) malignant lesions including 129/153 (84%) lymph nodes, 97/107 (91%) liver lesions, 25/72 (35%) lung lesions, and 24/42 (57%) "other" lesions (Table 2). 28/303 (9%) lesions were regarded as false-positive lesions. No significant difference was observed regarding the overall detection rate as compared to side-by-side analysis ($p=.73$). However, significant differences were still evident as compared to solely using wbDWI ($p=.01$) and wbT2 images ($p=.0001$), respectively.

Patient based diagnostic accuracy of fused images was similar to side-by-side analysis and yielded a sensitivity of 96% (95% CI: 89–100; 46/48), a specificity of 75% (95% CI: 50–99; 12/16), and an accuracy of 91% (95% CI: 82–98; 58/64, Table 3) using PET/CT as a reference standard. Fused images did not improve

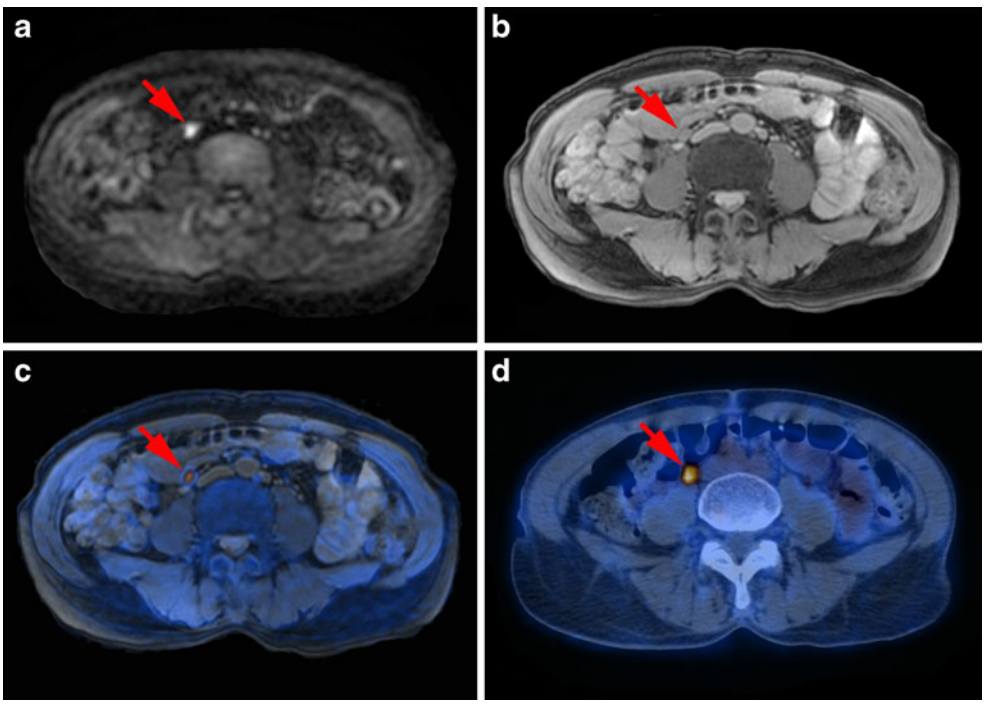

Fig. 3 A 59-year-old female patient with retroperitoneal lymph node metastases from cholangiocarcinoma. **a** WbDWI showed a hyperintense lesion (*arrow*) in the right lower abdomen that was missed by both investigators. **b** Interpretation of wbT2 alone did not allow correct lesion detection. Both side-by-side analysis (**a**+**b**) and image fusion (**c**) correctly depicted the malignant lymph node metastases in comparison to PET/CT (**d**)

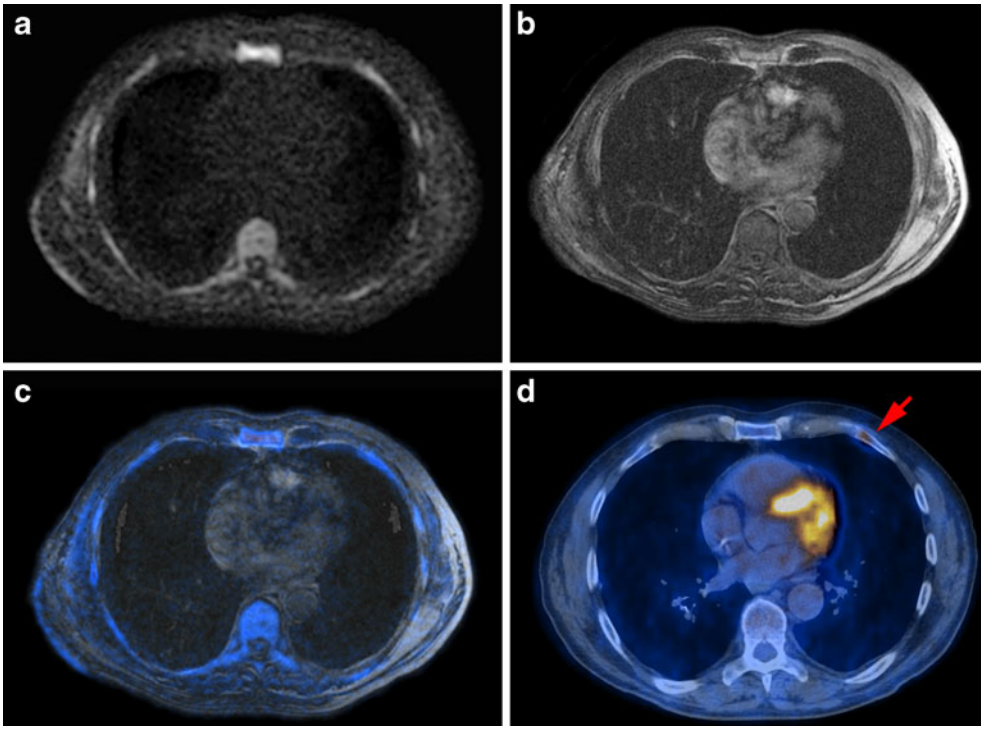

Fig. 4 A 69-year-old male patient with metastases in the rib from colorectal cancer. WbDWI (**a**), wbT2(**b**), and fused images (**c**) showed no evidence of malignant lesion. This lesion was missed on wbDWI, wbT2, and fused images. The reference standard PET/CT showed clear FDG-uptake in a left anterior rib consistent with an osseous metastasis (**d**)

(p=.76) the diagnostic accuracy as compared to side-by-side analysis.

Discussion

The results presented herein indicate that wbDWI allows detection of malignant lesions with similar accuracy to wbT2. Side-by-side analysis significantly improved the overall detection rate compared with the evaluation of wbT2 and wbDWI images separately. Additional assessment of fused images showed no significant improvement compared with side-by-side analysis for both lesion-based and patient-based assessment.

Concerning wbDWI, there was an overall detection rate of 64% and a patient-based diagnostic accuracy of 82%, which is consistent with recent studies evaluating detection of non-small cell lung cancer metastases [18] or breast cancer [19]. Other studies showed a higher diagnostic performance using DWI for distinct tumour entities like colorectal and pancreatic adenocarcinoma [20, 21] or endometrial cancer [22], which might be due to the use of organ-specific protocols compared with a wbDWI protocol. Lymph nodes accounted for many false-positive lesions in wbDWI. This may be attributable to the generally high signal intensity of lymph nodes in DWI and the lack of standardisation in lymph node interpretation using DWI [23]. We evaluated lymph nodes by comparing the relative signal intensity of suspect nodes with that of certainly benign lymph nodes as previously recommended [14]. Various other attempts however have been made for diffusion-weighted imaging as regards lymph node evaluation using visual assessment [24], size measurements [25] and absolute ADC measurements [26].

WbT2, derived from FIESTA, yielded a detection rate of 57% with a high PPV (93%), which is comparable to the diagnostic accuracy of other T2-weighted whole-body sequences like STIR [3, 27]. Our findings extend the findings of Bhosale et al. [28] who have already demonstrated the feasibility of FIESTA for oncological body imaging. Furthermore, this was performed without the use of contrast media, which has also been proposed for whole-body imaging to evaluate malignancy [5, 29].

In our study, the detection rate for malignant liver lesions was lower for wbT2 than for wbDWI. This reflects the findings of a study showing that DWI is more sensitive than T2-weighted imaging for the detection of hepatic metastases [30]. On the other hand, wbDWI showed a low PPV of 86.7% compared with wbT2, which may be caused through either incorrect lesion localisation due to limited spatial resolution of wbDWI or T2-shine-through effects. Most false-negative results were accounted for by lung metastases in both wbT2 and wbDWI, which indicates a limited capability for metastases detection in the lung and probably reflects the advantage of CT within PET/CT.

Side-by-side analysis improved the overall detection rate significantly instead of analysing wbT2 and wbDWI images separately, thus underlining the incremental value of the combined image interpretation. This is consistent with a study showing a significant increase in diagnostic

accuracy for detection of small cell lung cancer metastases when adding anatomical whole-body MRI sequences to wbDWI [18]. There is also evidence of an increased overall accuracy evaluating local malignant tumour spread in urinary bladder cancer for side-by-side analysis compared with interpretation of DWI and T2-weighted images alone [31]. Our results may carry forward those experiences from local tumour analysis to whole-body imaging.

WbT2/wbDWI image fusion shows significantly higher detection rates compared with wbT2 and wbDWI alone, which parallels findings from retrospective image fusion studies of DWI and T2-weighted image data [31–33]. However, these studies did not evaluate side-by-side analysis. In our patient cohort, the addition of fused images could not improve detection rates when compared with side-by-side assessment alone. Experiences from PET/CT fusion have shown an additional value of fused image data in comparison to side-by-side analysis [34, 35]. The fact, that we did not demonstrate a significant diagnostic improvement by image fusion might be due to the better spatial resolution of wbDWI at *b*-value 700 s/mm^2 compared with the spatial resolution of PET.

Study limitations

We did not use a *b*-value of 1,000 s/mm^2, which is the most common *b*-value for wbDWI and might yield superior body background suppression compared with a *b*-value of 700 s/mm^2. However, the use of a lower *b*-value yields a superior signal to noise ratio and spatial resolution and might therefore be advantageous in detecting small lesions. We did not perform cardiac triggering or respiratory triggering for wbDWI (which may have reduced signal loss and image blurring, respectively) limiting evaluation of the left hepatic lobe, the mediastinum and the lung [10]. WbDWI image slices were relatively thick (7 mm) with 1 mm gaps . We evaluated a heterogeneous patient population with different malignancies in this study; the population may also have a selection bias due to the distribution of malignancies. We investigated tumour detection using relative ADC measurements and did not use absolute ADC measurements for tumour characterisation. We used a built-in body coil for the head, neck and lower extremity with inferior contrast-to-noise ratio compared with a surface coil. PET/CT was used as a reference standard comprising limitations for detection of distinct tumour entities itself.

Conclusion

Using PET/CT as reference standard, wbDWI allows detection of malignant lesions with a similar detection rate to wbT2. Side-by-side analysis of wbT2 and wbDWI significantly improves the overall detection rate and fused image data interpretation provides no added value.

References

1. Bar-Shalom R, Yefremov N, Guralnik L et al (2003) Clinical performance of PET/CT in evaluation of cancer: additional value for diagnostic imaging and patient management. J Nucl Med 44:1200–1209
2. von Schulthess GK, Steinert HC, Hany TF (2006) Integrated PET/CT: current applications and future directions. Radiology 238:405–422. doi:10.1148/radiol.2382041977
3. Kavanagh E, Smith C, Eustace S (2003) Whole-body turbo STIR MR imaging: controversies and avenues for development. Eur Radiol 13:2196–2205. doi:10.1007/s00330-003-1890-z
4. Hargaden G, O'Connell M, Kavanagh E, Powell T, Ward R, Eustace S (2003) Current concepts in whole-body imaging using turbo short tau inversion recovery MR imaging. AJR Am J Roentgenol 180:247–252
5. Schmidt GP, Reiser MF, Baur-Melnyk A (2009) Whole-body MRI for the staging and follow-up of patients with metastasis. Eur J Radiol 70:393–400. doi:10.1016/j.ejrad.2009.03.045
6. Johnston C, Brennan S, Ford S, Eustace S (2006) Whole body MR imaging: applications in oncology. Eur J Surg Oncol 32:239–246. doi:10.1016/j.ejso.2005.09.018
7. Takahara T, Imai Y, Yamashita T, Yasuda S, Nasu S, Van Cauteren M (2004) Diffusion weighted whole body imaging with background body signal suppression (DWIBS): technical improvement using free breathing, STIR and high resolution 3D display. Radiat Med 22:275–282
8. Koh DM, Collins DJ (2007) Diffusion-weighted MRI in the body: applications and challenges in oncology. AJR Am J Roentgenol 188:1622–1635. doi:10.2214/AJR.06.1403
9. Kwee TC, Takahara T, Ochiai R et al (2009) Whole-body diffusion-weighted magnetic resonance imaging. Eur J Radiol 70:409–417. doi:10.1016/j.ejrad.2009.03.054
10. Naganawa S, Kawai H, Fukatsu H et al (2005) Diffusion-weighted imaging of the liver: technical challenges and prospects for the future. Magn Reson Med Sci 4:175–186
11. Hany TF, Steinert HC, Goerres GW, Buck A, von Schulthess GK (2002) Improvement of diagnostic accuracy of PET imaging using an in-line PET-CT system: preliminary results. J Nucl Med 43:307p–307p
12. Koh DM, Takahara T, Imai Y, Collins DJ (2007) Practical aspects of assessing tumors using clinical diffusion-weighted imaging in the body. Magn Reson Med Sci 6:211–224
13. Wahl RL, Jacene H, Kasamon Y, Lodge MA (2009) From RECIST to PERCIST: evolving considerations for PET response criteria in solid tumors. J Nucl Med 50(Suppl 1):122S–150S. doi:10.2967/jnumed.108.057307
14. Whittaker CS, Coady A, Culver L, Rustin G, Padwick M, Padhani AR (2009) Diffusion-weighted MR imaging of female pelvic tumors: a pictorial review. Radiographics 29:759–774, discussion 774–758 doi:10.1148/rg.293085130
15. Mentzel HJ, Kentouche K, Sauner D et al (2004) Comparison of whole-body STIR-MRI and 99mTc-methylene-diphosphonate scintigraphy in children with suspected multifocal bone lesions. Eur Radiol 14:2297–2302
16. Dorfman RE, Alpern MB, Gross BH, Sandler MA (1991) Upper abdominal lymph nodes: criteria for normal size determined with CT. Radiology 180:319–322

17. Glazer GM, Gross BH, Quint LE, Francis IR, Bookstein FL, Orringer MB (1985) Normal mediastinal lymph nodes: number and size according to American Thoracic Society mapping. AJR Am J Roentgenol 144:261–265
18. Ohno Y, Koyama H, Onishi Y et al (2008) Non-small cell lung cancer: whole-body MR examination for M-stage assessment—utility for whole-body diffusion-weighted imaging compared with integrated FDG PET/CT. Radiology 248:643–654. doi:10.1148/radiol.2482072039
19. Heusner TA, Kuemmel S, Koeninger A et al (2010) Diagnostic value of diffusion-weighted magnetic resonance imaging (DWI) compared to FDG PET/CT for whole-body breast cancer staging. Eur J Nucl Med Mol Imaging 37(6):1077–1086. doi:10.1007/s00259-010-1399-z
20. Ichikawa T, Erturk SM, Motosugi U et al (2006) High-B-value diffusion-weighted MRI in colorectal cancer. AJR Am J Roentgenol 187:181–184. doi:10.2214/AJR.05.1005
21. Ichikawa T, Erturk SM, Motosugi U et al (2007) High-b value diffusion-weighted MRI for detecting pancreatic adenocarcinoma: preliminary results. AJR Am J Roentgenol 188:409–414. doi:10.2214/AJR.05.1918
22. Tamai K, Koyama T, Saga T et al (2007) Diffusion-weighted MR imaging of uterine endometrial cancer. J Magn Reson Imaging 26:682–687. doi:10.1002/jmri.20997
23. Vilanova JC, Barcelo J (2008) Diffusion-weighted whole-body MR screening. Eur J Radiol 67:440–447. doi:10.1016/j.ejrad.2008.02.040
24. Ono K, Ochiai R, Yoshida T et al (2009) Comparison of diffusion-weighted MRI and 2-[fluorine-18]-fluoro-2-deoxy-D-glucose positron emission tomography (FDG-PET) for detecting primary colorectal cancer and regional lymph node metastases. J Magn Reson Imaging 29:336–340. doi:10.1002/jmri.21638
25. Nomori H, Mori T, Ikeda K et al (2008) Diffusion-weighted magnetic resonance imaging can be used in place of positron emission tomography for N staging of non-small cell lung cancer with fewer false-positive results. J Thorac Cardiovasc Surg 135:816–822. doi:10.1016/j.jtcvs.2007.10.035
26. Lin G, Ho KC, Wang JJ et al (2008) Detection of lymph node metastasis in cervical and uterine cancers by diffusion-weighted magnetic resonance imaging at 3T. J Magn Reson Imaging 28:128–135. doi:10.1002/jmri.21412
27. Lauenstein TC, Freudenberg LS, Goehde SC et al (2002) Whole-body MRI using a rolling table platform for the detection of bone metastases. Eur Radiol 12:2091–2099. doi:10.1007/s00330-002-1344-z
28. Bhosale P, Ma JF, Choi HS (2009) Utility of the FIESTA pulse sequence in body oncologic imaging: review. Am J Roentgenol 192:S83–S93. doi:10.2214/Ajr.07.7062
29. Schmidt GP, Baur-Melnyk A, Haug A et al (2009) Whole-body MRI at 1.5 T and 3 T compared with FDG-PET-CT for the detection of tumour recurrence in patients with colorectal cancer. Eur Radiol 19:1366–1378. doi:10.1007/s00330-008-1289-y
30. Bruegel M, Rummeny EJ (2009) Hepatic metastases: use of diffusion-weighted echo-planar imaging. Abdom Imaging. doi:10.1007/s00261-009-9541-8
31. Takeuchi M, Sasaki S, Ito M et al (2009) Urinary bladder cancer: diffusion-weighted MR imaging—accuracy for diagnosing T stage and estimating histologic grade. Radiology 251:112–121. doi:10.1148/radiol.2511080873
32. Tsushima Y, Takano A, Taketomi-Takahashi A, Endo K (2007) Body diffusion-weighted MR imaging using high b-value for malignant tumor screening: usefulness and necessity of referring to T2-weighted images and creating fusion images. Acad Radiol 14:643–650. doi:10.1016/j.acra.2007.02.006
33. Lin G, Ng KK, Chang CJ et al (2009) Myometrial invasion in endometrial cancer: diagnostic accuracy of diffusion-weighted 3.0-T MR imaging—initial experience. Radiology 250:784–792. doi:10.1148/radiol.2503080874
34. Metser U, Golan O, Levine CD, Even-Sapir E (2005) Tumor lesion detection: when is integrated positron emission tomography/computed tomography more accurate than side-by-side interpretation of positron emission tomography and computed tomography? J Comput Assist Tomogr 29:554–559
35. Antoch G, Saoudi N, Kuehl H et al (2004) Accuracy of whole-body dual-modality fluorine-18-2-fluoro-2-deoxy-D-glucose positron emission tomography and computed tomography (FDG-PET/CT) for tumor staging in solid tumors: comparison with CT and PET. J Clin Oncol 22:4357–4368. doi:10.1200/JCO.2004.08.120